Scripta Materialia 229 (2023) 115371

Contents lists available at ScienceDirect

Scripta Materialia

journal homepage: www.journals.elsevier.com/scripta-materialia

A Co-rich chemically complex intermetallic alloy with extraordinary strength-ductility synergy

Y.L. Zhao [a,*], W.C. Xiao [b], Z.K. Zhao [a], Q. Li [b], J. Cui [a], J.H. Luan [b], C.T. Liu [b,c], P.K. Liaw [d], T. Yang [b,c,**]

[a] School of Materials Science and Engineering, Harbin Institute of Technology (Shenzhen), Shenzhen 518055, China
[b] Department of Materials Science and Engineering Mechanical Behavior Division of Shenyang National Laboratory for Materials Science, City University of Hong Kong, Hong Kong, China
[c] Hong Kong Branch of National Precious Metals Material Engineering Research Centre (NPMM), City University of Hong Kong, Hong Kong, China
[d] Department of Materials Science and Engineering, The University of Tennessee, Knoxville, TN 37996-2200, USA

ARTICLE INFO

Keywords:
High-entropy alloy
Intermetallic compound
Mechanical properties
Work hardening
Grain-boundary engineering

ABSTRACT

High-strength ordered intermetallic alloys are always sought-after in sophisticated structural applications. However, their practical applications have long been hindered by the severe grain-boundary embrittlement. Here, we designed a Co-rich chemically complex intermetallic alloy (CCIMA) with the $L1_2$-type ordered structure, which exhibits an ultrahigh tensile strength of ~1,611 MPa and a substantial ductility of ~37%. These exceptional strength-ductility combination outperforms the majority of common Co-rich intermetallic alloys. The multi-addition of Ta, Ti, and V elements is largely responsible for the significantly increased antiphase boundary energy of the $L1_2$ superlattice, which accounts for the high strength. This high degree of ductility is attributed to both the increased fracture resistance of grain boundaries brought about by co-segregation-induced order-to-disorder phase transformation, as well as the high work-hardening capability.

Intermetallic alloys with the $L1_2$-ordered crystal structure provide enormous advantages over conventional disordered alloys for serving as high-temperature structural components in the aerospace and power generation. In particular, the long-range ordered (LRO) crystal structure produces strong chemical bonding between elements, rendering a relatively low atomic mobility and unique dislocation dynamics in the materials, and thus, giving rise to an unusual yield-anomaly behavior at elevated temperatures [1,2]. However, most of the conventional polycrystalline intermetallic alloys exhibit severe grain-boundary embrittlement during tensile deformation, which reduces their fracture toughness and restricts their capacity to be fabricated [3].

Researchers have realized that this brittleness puzzle can be largely addressed through the subtle manipulation of microalloying and macroalloying adjustments [4–6]. For example, boron is found to be an effective cohesive element for the grain boundary in the binary Ni_3Al intermetallic alloy. Even a modest amount of the element (in ppm) can significantly improve the ductility of the alloys [7]. Whereas, it exhibits a marginal effect on alleviating the grain-boundary embrittlement of the Co_3Ti alloy deformed in air [8]. Instead, Liu et al.'s investigation revealed that the Co_3Ti alloy can be ductilized with the assistance of substitutional ternary elements, namely Fe [9], although its physical origin has not been fully understood yet. Nevertheless, the mechanical performances of most conventional $L1_2$ intermetallic alloys developed so far are still unsatisfactory. The discovery of intermetallic alloys with gigapascal strength and decent tensile ductility remains elusive, which severely restricts their widespread structural applications and creates a huge barrier to their commercialization.

Recently, a new class of alloying concept that consists of multi-principal-element alloys (also known as high-entropy alloys, HEAs, or chemically complex alloys) has produced a vast array of novel alloys with a variety of alluring properties [10–14], including superior mechanical performances, sluggish diffusion, good corrosion resistance, etc. Based on this concept, the realm of high-entropy materials has been extended to versatile categories [15]. In particular, the emerging chemically complex intermetallic alloys (CCIMAs) have attracted a great deal of attention due to their excellent mechanical properties and

* Corresponding author.
** Corresponding author at: Department of Materials Science and Engineering Mechanical Behavior Division of Shenyang National Laboratory for Materials Science, City University of Hong Kong, Hong Kong, China.
E-mail addresses: zhaoyilu@hit.edu.cn (Y.L. Zhao), taoyang6-c@my.cityu.edu.hk (T. Yang).

https://doi.org/10.1016/j.scriptamat.2023.115371
Received 14 November 2022; Received in revised form 14 February 2023; Accepted 14 February 2023
Available online 21 February 2023

enormous potential for high-temperature applications. For example, Yang et al. proposed an "interfacial disordered nanolayer (IDN) induced ductilization" approach in a interesting $L1_2$-type Ni-rich CCIMA, ($Ni_{43.9}Co_{22.4}Fe_{8.8}Al_{10.7}Ti_{11.7}B_{2.5}$, at.%) by delicately modulating the elemental synergism [16]. The underlying idea is to raise the antiphase boundary (APB) energy of the alloy by the addition of Ti element on one hand and form interfacial disordered nanolayers along the grain boundaries driven by a synergetic co-segregation behavior of Co, Fe, and B on the other hand. These together, consequently, enable a simultaneous increase in both the strength and ductility of this CCIMA, which readily override the properties of conventional Ni_3Al-type intermetallic alloys. The success of these efforts has rekindled the interest in the ordered intermetallic alloys and greatly encourages the creation of CCIMAs as a promising class of structural materials for high-temperature applications.

Nonetheless, compared to the Ni-rich intermetallic alloys developed so far, Co-rich intermetallic alloys are intuitively expected to achieve a higher upper limit of operation temperature due to the inherent advantage of pure Co on the melting temperature. This feature allows Co-rich materials to have higher melting points than the Ni-rich alloys by greater than 50 ~ 100 °C [17], rendering Co-rich intermetallic alloys great prospects for structural applications at elevated temperatures. Recently, Long et al. thoroughly exploited the potential of a $L1_2$-type Co-rich $(Co,Ni)_3(Al,W,Ti,Ta)$ CCIMA (denoted as L26 henceforth) to serve as a high-temperature structural material. Results showed that the L26 CCIMA exhibits decent high-temperature compressive strengths and a comparable creep property as Ni_3Al compounds, which preliminarily demonstrates the latent performance advantage of Co-rich CCIMAs for high-temperature applications [18]. However, to date, there are still few studies that have concentrated on the tensile properties and the related plastic-deformation mechanisms of those CCIMAs.

Here, we innovatively developed a Co-rich CCIMA by exploiting the IDN ductiliztion effect. A detailed investigation of the grain-boundary chemistry and structure, and their contribution to the mechanical properties will be conducted. Alloys with a nominal composition of $(Co_{47}Ni_{30}Al_{10}V_5Ta_4Ti_4)_{99}B_1$ (at.%, denoted as Co-rich CCIMA hereafter) were prepared by mixing high-purity materials (> 99.9%) in an arc-melting machine within an argon-filled environment. All ingots were repeatedly flipped over and remelted at least eight times to ensure chemical homogeneity, which was then cast into a sheet-shaped Cu mold surrounded by cooling water. The as-cast specimen was homogenized at 1150 °C for 24 h. Subsequently, a cycling process, including cold-rolling with a reduction ratio of ~20% and followed by annealing at 1150 °C for 15 mins, was performed until a total reduction of thickness reached ~66%. Dog-bone-shaped specimens with a gauge dimension of ~12.5 mm × 3.2 mm × 1 mm were machined from the well-crafted sheets by an electro-discharge machine. The surfaces of the tensile specimens were mechanically ground and then tested at a strain rate of $1.0 \times 10^{-3}s^{-1}$ using an Instron testing machine.

Microstructural analyses were performed by a field-emission scanning electron microscope (SEM) equipped with an electron-backscattered diffraction (EBSD, Oxford) detector. Phase characterization and deformation behavior were investigated by a JEM-2100F transmission electron microscope (TEM) operated at an acceleration voltage of 200 kV. Samples for SEM and EBSD characterizations were prepared by electro-polishing with an HNO_3 (~25%)/ CH_3OH (~75%) solution by volume under a direct voltage of 20 V at a temperature of −40 °C. A detailed chemical distribution across the grain boundary was quantitively examined by the atom probe tomography (APT) at 70 K in a voltage mode (200 kHz), and a pulse fraction of 20%.

Fig. 1 shows the microstructure of the designed Co-rich CCIMA. The SEM image (see Fig. 1a) and the EBSD inverse pole figure (IPF, see Fig. 1b) taken along the normal direction of the sample clearly reveal a non-textured equiaxed grain structure with an average grain size of 5.8 ± 0.7 μm. Also note that despite a small amount of randomly dispersed borides, no secondary precipitates can be detected in the present CCIMA.

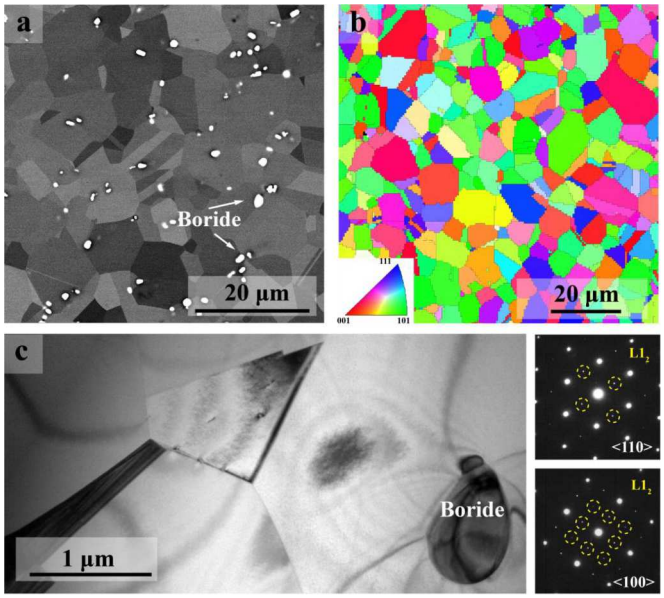

Fig. 1. Overall microstructures of the present Co-rich CCIMA. (a) typical SEM image, (b) EBSD inverse pole figure, and (c) typical TEM image and the corresponding selected diffraction (SAED) patterns of the grain interior with ⟨110⟩ and ⟨100⟩ zones. The faint superlattice diffraction spots that reflect the $L1_2$ structure are indicated by yellow dashed circle in the SAED patterns.

The structural features obtained from the TEM analysis, including the bright-field (BF) TEM image and the associated selected area diffraction (SAD) patterns acquired along ⟨100⟩ and ⟨110⟩ zone axes (see Fig. 1c), further demonstrated that the grain interior of this Co-rich CCIMA comprises a single $L1_2$ phase.

To reveal the microstructure and the chemical distribution near the vicinity of the grain boundary, both the high-resolution TEM (HRTEM) and APT were carefully performed. Excitingly, in addition to the $L1_2$ grain interior, an evident disordered face-centered-cubic (FCC) nanolayer is found near the grain boundary, which can be confirmed by the fast Fourier transform (FFT) image inserted on the up-right corner in Fig. 2a. This trend means that the IDN dutilization may be triggered at the present Co-rich CCIMA. Fig. 2b shows three-dimensional (3-D)

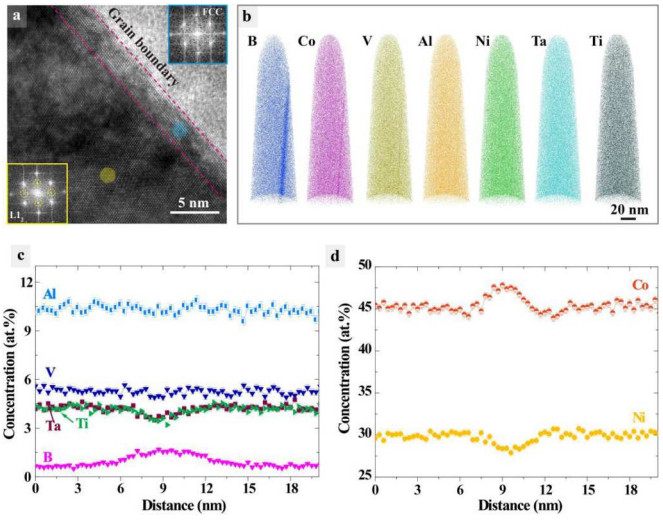

Fig. 2. (a) High-resolution TEM image and the insetted fast fourier transform (FFT) revealing the interfacial disordered nanolayer (IDN) formed at the grain boundary; (b) 3D reconstructions of individual element maps for an APT tip contains a grain boundary; (c) and (d) the corresponding chemical profile across the grain boundary, showing a co-segregation behavior of B and Co.

reconstructions of a typical APT tip taken from the present Co-rich CCIMA, where a near-edge-on grain boundary can be clearly visualized. From the individual atom maps in Fig. 2b, B shows substantial segregation, whereas Co segregates marginally. Fig. 2c and d further present the precise quantitative measurement of the chemical distributions across the grain boundary. The one-dimensional (1-D) concentration profiles obtained perpendicular to the grain-boundary plane indicated a co-segregation of Co and B at the grain boundary, concurrently with the depletion of Ni, Ti, and Ta. Other elements, such as Al and V, did not show any preferential segregation. The enrichment of B and Co can approximately rise by ~1 and 3 at.%, respectively, in comparison to the surrounding grain interior.

Fig. 3a displays the mechanical performance (tensile deformation) of the present Co-rich CCIMA at ambient temperature. As compared to the chemically simple Co-rich $L1_2$ intermetallic alloy (i.e., the Co_3Ti [19] and Co-12Al-11 W [20]) as well as the earlier multicomponent $L1_2$-type intermetallic alloy (i.e., the L26 intermetallic alloy) [18], our present Co-rich CCIMA exhibits outstanding tensile properties with both superior strength (yield strength of ~748 MPa and ultimate tensile strength of ~1611 MPa) and exceptionally large ductility (~37%). Generally, the strength of an $L1_2$ intermetallic alloy originates from the high resistance of deformation caused by the formation of APB domains, which increases with the APB energy. Archive literature shows that the APB energy (ΔE_{APB}) of the $L1_2$ phase in multicomponent Ni-based superalloys is very sensitive to the alloy composition. According to the study by Crudden et al., the APB energy can be calculated by superposing the contributions from individual alloying elements [21]:$\Delta E_{APB} = E^0_{APB} + \sum_i^n (k_i x_i)$, where E^0_{APB} is the APB energy of Ni_3Al, k_i and x_i are the correlation coefficient and concentration of the corresponding alloying elements (in at.%), respectively. Liang et al. further resolved the correlation coefficients for some commonly-alloyed elements based on theoretical calculations [22]. Their results revealed that both Ta and Ti elements have considerably large positive correlation coefficients (27.1 and 15, respectively) among those commonly-alloyed elements, such as W (4.6), demonstrating the effectiveness of these elements in increasing the APB energy [22]. Meanwhile, the addition of V to the current Co-rich CCIMA also plays an important role in strengthening materials. Given that V and Ti manifest the nearly identical linear compositional dependence with the APB energy [23], the correlation coefficient of V will be assumed to have the same value as Ti in the present work for the sake of simplicity. Based on the aforementioned equation, the APB energy of the present Co-rich CCIMA is estimated to be 413 mJ/m^2, which is significantly greater than that of the other alloys [24,25] displayed in Fig. 3a. Given that the critical shear stress for dislocation nucleation in an ordered $L1_2$ alloy has a positive correlation with its APB energy [26], this substantially increased APB energy driven by the addition of multiple positive elements (i.e., Ta, Ti, and V) in turn raise the barrier of dislocation movement and contributes to the high yield strength of the present Co-rich CCIMA.

The fracture surface of the present alloy is shown as the inset in Fig. 3a. Instead of intergranular fracture that is often shown in the conventional $L1_2$ alloys, transgranular fracture with numerous dimples is clearly observed, implying the ductile nature of the present alloy. The large ductility of polycrystalline materials relies principally on their strong load-bearing grain boundaries together with a high work-hardening capability [27]. Fig. 3b demonstrates the variation of strain-hardening rates (SHRs) with the applied true strain. Note that only the data from the uniform plastic deformation are used here for analysis. Three distinct stages can be evidenced in the SHR curves. In stage I, a dramatic drop in the SHR can be visible, which is correlated to the unnoticeable yielding plateau. Such a discontinuous yielding behavior is also frequently observed in many other ordered alloys subject to stretching [28,29]. Soon after the drop, an up-turn of the SHR is observed, followed by a gentle decrease till the true strain reaches ~10% (stage II). After that, interestingly, a second up-turn appears as the tensile deformation continues (stage III). Noticeably, the work-hardening rates of the present alloy are anomalously high (~5 GPa), as compared to the disordered alloys [30]. The strain-hardening exponent, n, is calculated, based on the constitutive law of $\sigma = k\varepsilon^n$, where σ and ε are the true stress and plastic strain, respectively. k is a scaling constant. As can be seen in Fig. 3c, the constant, n, varies with the true strain and surges to ~0.7 at stage III, which surpasses almost all the single-FCC HEA with a high fracture energy [31] and also TWIP/-TRIP steels [32,33], demonstrating a superb work-hardening capability.

To further reveal the plastic-deformation micro-mechanisms of the present Co-rich CCIMA, detailed EBSD and TEM analyses on the deformed specimen were conducted. Fig. 4a shows the typical TEM observations on the deformation substructures of the specimen deformed by a ~2% true plastic strain. An enlarged view of the region indicated in Fig. 4a was imaged by the weak-beam dark-field (WBDF) technique (see the inset), where superlattice dislocation pairs are clearly discernible. The separation distance between superlattice dislocation pairs is in the range of 2.5 ~ 6 nm. At the initial stage of plasticity, those

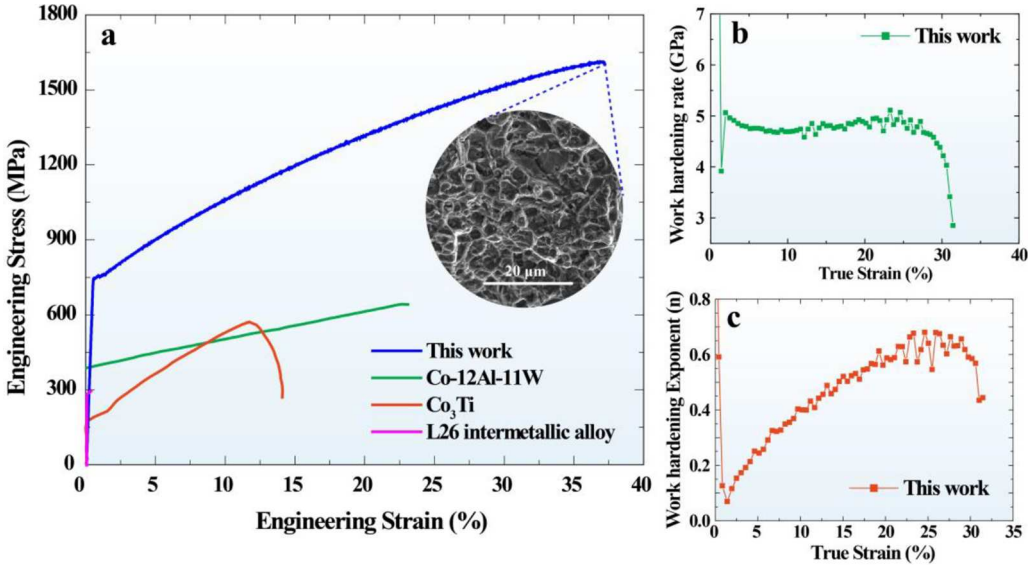

Fig. 3. (a) tensile properties of the present Co-rich CCIMA, compared with the well-studied Co-rich intermetallic alloys and the L26 CCIMA; (b) and (c) the corresponding work-hardening rate and the work-hardening exponent as a function of true strain, respectively.

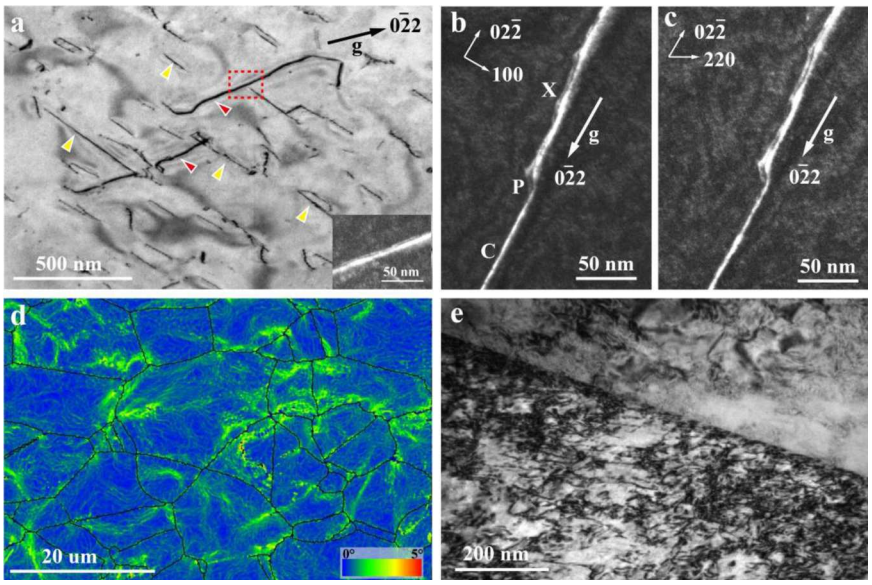

Fig. 4. (a) TEM images showing the dominated deformation substructure of the sample deformed by a ~2% plastic strain. The pair-wised feature of the superlattice dislocations is verified and shown as inset; (b) and (c) Weak-beam dark-field (WBDF) micrographs showing different dissociated behaviors of the segments (X, P, C) of the superlattice screw dislocations; (d) and (e) Kernel average misorientation (KAM) map and TEM image of the dislocations in the vicinity of the grain boundary revealing the strong load-bearing ability of the beneficial IDNs in the grain-boundary regions.

pair-wised superlattice dislocations serve as the dominant deformation carrier, which behaves in a similar fashion in the conventional $L1_2$-type intermetallic alloys for energy minimization [34]. Careful tilting experiments demonstrated that they have primary burgers vectors of $b = a/2[0\bar{1}1]$ and $b = a/2[\bar{1}10]$, highlighted by red and yellow arrows, respectively. To further reveal the dissociated behavior of the screw superlattice dislocations, trace analysis along the direction of the burgers vector was performed. An example of a superlattice dislocation pair under different tilting conditions is present in Fig. 4b and c. The variation of the separation distance between those superlattice dislocations during tilting manifests the segments X, P, C of this superlattice dislocation dissociated on different planes. With careful analysis, segment C of the superlattice dislocations appears to undergo a cube cross slip. This trend can be deduced as the dislocation tends to be overlapped when the cube cross-slip plane is projected nearly edge-on (see Fig. 4b). The other segments X and P are demonstrated to be dissociated on the $(\bar{1}11)$ and (111) planes, respectively. Another feature that is worth noting is the frequent occurrence of dislocation dipoles, which is considered to be the result of elastic interactions between the expanding dislocation loops or the dislocation reaction during their cross slip [35]. In fact, both screw and edge dipoles are frequently observed in the $L1_2$ alloys during plastic deformation, such as the Ni_3Al [36] and Ni_3Fe alloys [37], etc. Apropos of the deformation characterization (see Fig. 4), the specific explanation based on the APB tube mechanism [38,39] for the anomalous high work hardening is the lack of meaning, since no APB tube is observed in the present work. Given that the secondary slip systems have been already activated at the early stage of deformation (see Fig. 4), the mutual interactions of the superlattice dislocations activated in multiple slip systems and the associated jog dragging or/and kink locking in the wake of further straining can be expected, which will result in an additional frictional drag and make the major contribution to the exceptionally high work hardening in the present work [30]. Based on the Considere's criterion, such a high work-hardening capability help to postpone plastic (geometric) instability and promote a balanced mechanical property.

As the tensile stretching increases, massive dislocations mutually interacted and accumulated at the grain-boundary region. Fig. 4c shows the Kernel average misorientation (KAM) map taken from the fractured specimen. Evidently, most of the grain boundaries are surrounded by a higher density of geometry necessary dislocations (GNDs), also referred to by the high KAM value, implying that the plastic strain is considerably localized in the IDNs at grain boundaries. Fig. 4d presents a TEM image for the typical deformation substructures from the sample deformed by an ~31% true plastic strain, which reveals a pronounced dislocation activity in the IDN regions without forming detectable grain-boundary cleavages. This feature again manifests the considerable load-bearing capability of the beneficial disordered grain-boundary nanolayer.

Certainly, such a remarkable improved grain-boundary strength of the intermetallic alloys could be attributed to the elemental co-segregation behaviors through delicate atomic-scale grain-boundary engineering. In the present study, the role of B addition is mainly twofold. First, B is believed to increase the cohesive strength of the grain boundary of the Co-rich alloys [40], which, to some extent, facilitates an improved plastic ability. Second, it helps promote the segregation of Co element [16]. Since Co is traditionally viewed as a face-centered-cubic (FCC) stabilizer [41], the segregation of Co would degrade the ordering energy in the grain-boundary region, leading to a localized order-disorder transformation and resulting in the formation of IDN in that region (see Fig. 2). In contrast to the disordered FCC alloy, the specific atomic occupation behavior and the associated long-range ordered structure produce stronger chemical binding between atoms (i.e., ionic/covalent-like binding with a directional character). As such, it is generally assumed that the grain-boundary structures of a highly ordered alloy are considerably distorted [42], making it more prone to brittle fracture. As disordering ($L1_2$→FCC) occurs near the grain boundary, forming the IDNs with less distorted structure, the critical stress for dislocation nucleation and transmission can be substantially decreased, resulting in the ease of local shear and increasing dislocation motion and activities at grain boundary regions [43,44]. This would effectively relieve the local stress concentration raised by dislocation accumulation at grain boundaries and accommodate the plastic deformation compatibility for the adjacent grains. Additionally, the presence of INDs will also lower the stress for a dislocation emission from a crack tip, which helps to suppress the propagation of cracks at the interfaces accordingly. Collectively, the corresponding fracture resistance of this well-crafted CCIMA substantially increases, which shakes off the shackles of severe brittleness that are generally encountered in conventional polycrystalline intermetallic alloys. In strong contrast, though a co-segregation of Al and B elements can be clearly observed in the L26 CCIMA [18], the alloy exhibits extreme brittleness ($< 0.42\%$) under mechanical straining. This could be related to the segregation of Al element. Such a segregation creates a nearly ideal stoichiometric composition (A_3B-type) in the vicinity of the grain boundary, which is expected to increase the ordering energy and the associated distortion for an enhanced brittle tendency [42]. More specifically, on account of

the electronegativity difference of the A and B elements in an A_3B-type ordered alloy, the B atom generally has a strong tendency to draw charge from the A atom, leaving less charge participating in the A-A bonds nearby. Since the A-A bond is assumed to be the major bond at the grain boundary, the reduction of charge density results in a decreased grain-boundary cohesion [45]. In other words, the increased ordering energy in the grain-boundary region tends to aggravate charge hetero-distribution, leading to weakened grain boundaries accordingly [45]. These two distinctive scenarios suggest that the grain-boundary chemistry and the associated disordered nanolayer formed at the grain boundary hold the key to the improved ductility. The deviation of the elemental segregation tendency in the two cases could be associated with the different segregation enthalpy of elements in their surroundings [46]. Jin et al. reported that W holds a stronger bonding strength with Co than that of Co-Al pairs [47]. One can expect that the relatively weak bonded element (Al) may have a higher chance to segregate and occupy the grain-boundary site for a reduced energy. Yet the physical origins of the segregation tendency of elements in CCIMA systems remain unclear at the present. More detailed studies especially with the assistance of theoretical studies will be necessary to further clarification.

In summary, we designed and successfully fabricated a Co-rich $L1_2$-type chemically complex intermetallic alloy (CCIMA) with interfacial disordered nanolayers formed at grain boundaries. This intriguing architecture enables these CCIMA to have a superior mechanical property that overrides most of the conventional Co-rich intermetallic alloys. Specifically, the multi-additions of Ta, Ti, and V elements are demonstrated to substantially increase the antiphase-boundary energy, leading to an elevated impediment for dislocation motion and an increased strength consequently. The large ductility in our CCIMA at such a high strength level could be attributed to the combined effect of the high work-hardening ability and increased fracture resistance raised by IDNs at grain boundaries. Detailed analysis of the deformed microstructure revealed that the high work-hardening capability of the present CCIMA could be attributed to the mutual interaction of superlattice dislocations from multiple slip systems and their associated dragging effect. Besides, driven by the elemental co-segregation of Co and B elements, the disordered nanolayers produce a relatively undistorted grain-boundary regions and allow greater freedom for dislocation activities to occur, thereby enhancing the fracture resistance of the alloy without grain-boundary embrittlement. This study provides insight into the micromechanism of the deformation behaviors of the CCIMA and will offer the guidance for the development of the CCIMA with enhanced mechanical properties for high-temperature applications.

Declaration of Competing Interest

The authors declare that they have no known competing financial interests or personal relationships that could have appeared to influence the work reported in this paper.

Acknowledgment

The authors from the Harbin Institute of Technology (Shenzhen) thank the financial support from the National Natural Science Foundation of China (Grant No. 52101135) and the Shenzhen Science and Technology Program (Grant No. RCBS20210609103202012). The authors from the City University of Hong Kong greatly acknowledge the financial supports from the National Natural Science Foundation of China (Grant Nos. 52101151 and 52222112) and the Shenzhen Science and Technology Program (Grant No. SGDX20210823104002016). P.K. L. acknowledges support from (1) the Army Office Projects (Grant Nos. W911NF-13- 1–0438 and W911NF-19–2-0049) with program managers, Michael P. Bakas, David M. Stepp, and S. Mathaudhu and (2) the National Science Foundation (Grant Nos. DMR-1611180 and 1809640) with program directors, Jonathan Madison, Judith Yang, Gary Shiflet, and Diana Farkas. All the authors declare that they have no known competing financial interests or personal relationships that could have appeared to influence the work reported in this paper.

References

[1] N.S. Stoloff, Ordered alloys for high temperature applications, Mater. Res. Soc. Symp. Proc. 39 (1985) 3–27.
[2] C.T. Liu, Recent advances in ordered intermetallics, Mater. Chem. Phys. 288 (1993) 3–19.
[3] C.T. Liu, Ductility and fracture behavior of polycrystalline Ni3Al alloys, Mater. Res. Soc. Symp. Proc. 81 (1987) 355–367.
[4] C.T. Liu, Grain-boundary design of L12 ordered intermetallic alloys, MRS Online Proc. Libr. 122 (1988) 429.
[5] K. Aoki, Ductilization of L12 intermetallic compound Ni3Al by microalloying with boron, Mater. Trans. JIM 31 (1990) 443–448.
[6] A. Chiba, S. Hanada, S. Watanabe, Ductilization of Ni3Al by macroalloying with Pd, Acta Metall. Mater. 39 (1991) 1799–1805.
[7] C.T. Liu, C.L. White, J.A. Horton, Effect of boron on grain-boundaries in Ni3Al, Acta Metall. 33 (1985) 213–229.
[8] T. Takasugi, M. Takazawa, O. Izumi, Environmental effects on the mechanical properties of Co3Ti containing boron, carbon and beryllium, J. Mater. Sci. 25 (1990) 4239–4246.
[9] Y. Liu, T. Takasugi, O. Izumi, H. Suenaga, Mechanical properties of Co3Ti polycrystals alloyed with various additions, J. Mater. Sci. 24 (1989) 4458–4466, 1989 2412.
[10] E.P. George, D. Raabe, R.O. Ritchie, High-entropy alloys, Nat. Rev. Mater. 4 (2019) 515–534, 2019 48.
[11] D.B. Miracle, O.N. Senkov, A critical review of high entropy alloys and related concepts, Acta Mater. 122 (2017) 448–511.
[12] J.W. Yeh, S.K. Chen, S.J. Lin, J.Y. Gan, T.S. Chin, T.T. Shun, C.H. Tsau, S.Y. Chang, Nanostructured high-entropy alloys with multiple principal elements: novel alloy design concepts and outcomes, Adv. Eng. Mater. 6 (2004) 299–303.
[13] B. Cantor, I.T.H. Chang, P. Knight, A.J.B. Vincent, Microstructural development in equiatomic multicomponent alloys, Mater. Sci. Eng. A 375–377 (2004) 213–218.
[14] Y. Zhang, T.T. Zuo, Z. Tang, M.C. Gao, K.A. Dahmen, P.K. Liaw, Z.P. Lu, Microstructures and properties of high-entropy alloys, Prog. Mater. Sci. 61 (2014) 1–93.
[15] C. Oses, C. Toher, S. Curtarolo, High-entropy ceramics, Nat. Rev. Mater. 5 (2020) 295–309, 2020 54.
[16] T. Yang, Y.L. Zhao, W.P. Li, C.Y. Yu, J.H. Luan, D.Y. Lin, L. Fan, Z.B. Jiao, W.H. Liu, X.J. Liu, J.J. Kai, J.C. Huang, C.T. Liu, Ultrahigh-strength and ductile superlattice alloys with nanoscale disordered interfaces, Science 369 (2020) 427–432.
[17] A. Suzuki, H. Inui, T.M. Pollock, L12-strengthened cobalt-base superalloys, Annu. Rev. Mater. Res. 45 (2015) 345–368.
[18] F.R. Long, S.I. Baik, D.W. Chung, F. Xue, E.A. Lass, D.N. Seidman, D.C. Dunand, Microstructure and creep performance of a multicomponent Co-based L12–ordered intermetallic alloy, Acta Mater. 196 (2020) 396–408.
[19] T. Takasugi, O. Izumi, Electronic and structural studies of grain boundary strength and fracture in L12 ordered alloys-I. on binary A3B alloys, Acta Metall. 33 (1985) 1247–1258.
[20] T. Oohashi, N.L. Okamoto, K. Kishida, K. Tanaka, H. Inui, Microstructures and mechanical properties of Co3(Al,W) with the L12 structure, Mater. Res. Soc. Symp. Proc. 1128 (2009) 221–226.
[21] D.J. Crudden, A. Mottura, N. Warnken, B. Raeisinia, R.C. Reed, Modelling of the influence of alloy composition on flow stress in high-strength nickel-based superalloys, Acta Mater. 75 (2014) 356–370.
[22] Z. Liang, J.D.H. Paul, A. Stark, A. Bezold, S. Neumeier, M. Göken, F. Pyczak, High-temperature CoNi-based superalloys strengthened by γ′-(Ni,Co)3(Cr,Al,Ti,X): the Effect of refractory elements, Metall. Mater. Trans. A (2022) 1–15.
[23] O.I. Gorbatov, I.L. Lomaev, Y.N. Gornostyrev, A.V. Ruban, D. Furrer, V. Venkatesh, D.L. Novikov, S.F. Burlatsky, Effect of composition on antiphase boundary energy in Ni3Al based alloys: ab initio calculations, Phys. Rev. B 93 (2016) 224106.
[24] N.M. Rosengaard, H.L. Skriver, Ab. initio study of antiphase boundaries and stacking faults in Llq and DO&z compounds, Phys. Rev. B 50 (1994) 15–1994 (n. d.).
[25] K.V. Vamsi, S. Karthikeyan, Yield anomaly in L12 Co3AlxW1−x vis-à-vis Ni3Al, Scr. Mater. 130 (2017) 269–273.
[26] I. Baker, B. Huang, E.M. Schulson, The effect of boron on the lattice properties of Ni3Al, Acta Metall. 36 (1988) 493–499.
[27] M.A. Meyers, K.K. Chawla, Mechanical Behavior of Materials, Cambridge University Press, 2008.
[28] E.M. Schulson, T.P. Weihs, D.V. Viens, I. Baker, The effect of grain size on the yield strength of Ni3Al, Acta Metall. 33 (1985) 1587–1591.
[29] E.M. Schulson, J.A. Roy, The yield strength of the L12 phase Zr3Al, Acta Metall. 26 (1978) 29–38.
[30] Y.Q. Sun, P.M. Hazzledine, Dislocations in Solids-Chapter 49 Geometry of Dislocation Glide in Ll2 γ′-phase: TEM Observations, Elsevier Science Publishers B. V., 1996.
[31] B. Gludovatz, A. Hohenwarter, K.V.S. Thurston, H. Bei, Z. Wu, E.P. George, R. O. Ritchie, Exceptional damage-tolerance of a medium-entropy alloy CrCoNi at cryogenic temperatures, Nat. Commun. 7 (2016) 1–8.
[32] H. Ding, H. Ding, D. Song, Z. Tang, P. Yang, Strain hardening behavior of a TRIP/TWIP steel with 18.8% Mn, Mater. Sci. Eng. A 528 (2011) 868–873.

[33] L. Qian, K. Li, F. Huang, D. Li, T. Wang, J. Meng, F. Zhang, Enhancing both strength and ductility of low-alloy transformation-induced plasticity steel via hierarchical lamellar structure, Scr. Mater. 183 (2020) 96–101.
[34] B.H. Kear, Dislocation configurations and work hardening in Cu3Au crystals, Acta Metall. 12 (1964) 555–569.
[35] F.R.N. Nabarro, M.S. Duesbery, Dislocations in Solid, 10, Elsevier, 1996.
[36] H.P. Karnthaler, E.T. Mtjhlbacher, C. Rentenberger, The influence of the fault energies on the anomalous mechanical behaviour of Ni3Al alloys, Acta Mater. 44 (1996) 547–560.
[37] A. Korner, H.P. Karnthaler, C. Hitzenberger, Transmission electron microscopy study of cross-slip and of Kear-Wilsdorf locks in L12 ordered Ni3Fe, Philos. Mag. A Phys. Condens. Matter Struct. Defects Mech. Prop. 56 (1987) 73–88.
[38] A.E. Vidoz, L.M. Brown, On work-hardening in ordered alloys, Philos. Mag. 7 (1962) 1167–1175.
[39] P.M. Hazzledine, Y.Q. Sun. The strain field and work-hardening from antiphase boundary tubes in ordered alloys, High Temp. Alum, Elsevier, 1992, pp. 189–194.
[40] G. Lu, J.T. Guo, K.Y. Chen, Z.Q. Hu, A first principles investigation of environmental embrittlement of Co3Ti alloy, Acta Mater. 44 (1996) 4019–4045.
[41] S. Lu, S. Antonov, L. Li, C. Liu, X. Zhang, Y. Zheng, H.L. Fraser, Q. Feng, Atomic structure and elemental segregation behavior of creep defects in a Co-Al-W-based single crystal superalloys under high temperature and low stress, Acta Mater. 190 (2020) 16–28.
[42] J.J. Kruisman, V. Vitek, J.T.M. De Hosson, Atomic structure of stoichiometric and non-stoichiometric grain boundaries in A3B compounds with L12 structure, Acta Metall. 36 (1988) 2729–2741.
[43] B.J. Pestman, J.T.M. De Hosson, V. Vitek, F.W. Schapink, Interaction between lattice dislocations and grain boundaries in f.c.c. and ordered compounds: a computer simulation, Philos. Mag. A 64 (2006) 951–969.
[44] B.J. Pestman, J.T.M. de Hosson, Interactions between lattice dislocations and grain boundaries in Ni3Al investigated by means of in situ TEM and computer modelling experiments, Acta Metall. Mater. 40 (1992) 2511–2521.
[45] O. Izumi, T. Takasugi, Mechanisms of ductility improvement in L12 compounds, J. Mater. Res. 3 (1988) 426–440.
[46] M. Wagih, P.M. Larsen, C.A. Schuh, Learning grain boundary segregation energy spectra in polycrystals, Nat. Commun. 11 (2020) 1–9, 2020 111.
[47] M. Jin, N. Miao, W. Zhao, J. Zhou, Q. Du, Z. Sun, Structural stability and mechanical properties of Co3(Al, M) (M = Ti, V, Cr, Zr, Nb, Mo, Hf, Ta, W) compounds, Comput. Mater. Sci. 148 (2018) 27–37.